Development of a Gas-Puff Z-Pinch for the MAIZE Linear Transformer Driver

A. P. Shah, *Member, IEEE*, B. J. Sporer, G. V. Dowhan, *Member, IEEE*, K. W. Elliott, M. Krishnan, N. M. Jordan, *Senior Member, IEEE*, and R. D. McBride, *Member, IEEE*

***Abstract*— A gas-puff z-pinch experimental platform has been developed for the 0.5–1-MA, 100–250-ns MAIZE pulsed power facility at the University of Michigan. The experiment consists of a nozzle and fast-valve assembly, which is integrated into the pulsed power circuit and forms a gas load in the center of the pulsed power device. The capacitors that form the pulsed power device discharge through the gas, forcing it to pinch on axis. Such a gas-puff z-pinch is afflicted by various instabilities, the mitigation of which is achieved by imploding multiple concentric shells of gas with increasing gas density toward the center of the pinch and imploding high mass number gases onto low mass number gases. These constraints suggested the development of a triple-nozzle system with an outer shell, inner shell, and central jet. A voltage-driven thin-shell model was used to inform the design of the gas-puff nozzles' radii and gas pressures in the fast valve. The hardware was developed based on this point design. The MAIZE transmission lines were redesigned to accommodate the new hardware. Systems that support the gas-puff experiment include a gas manifold that supplies the nozzles with gas; a driver that pulses the valve to opened and closed states; and a logic circuit that provides a signal if and only if the gas-puff load successfully forms, to trigger MAIZE and the diagnostics. These were all constructed, tested, and integrated into the experiment. Additional diagnostics were also developed and fielded: a 2-D interferometer, a four polycrystalline diamond (PCD) detector array with Ross filter pairs, and neutron bubble detectors. Characteristic results from the first z-pinch experiments conducted with this gas-puff system are presented. The system demonstrates an x-ray energy output of up to 720 $\pm$ 50 J per pulse and a neutron output of up to $(4.9 \pm 0.5) \times 10^8$ neutrons per pulse. Notably, this system has enabled shot rates of over 30 z-pinch experiments per day on MAIZE.**

***Index Terms*— K-shell x-ray source, neutron source, Z-pinch plasmas.**

Manuscript received 10 October 2023; revised 10 March 2024 and 17 June 2024; accepted 6 July 2024. This work was supported in part by a seed grant from the Michigan Memorial Phoenix Project, in part by the DOE Early Career Research Program under Grant DE-SC0020239, and in part by DOE-NNSA through the SSAA Program under Cooperative Agreements DE-NA0003764 and DE-NA0004148. The review of this article was arranged by Senior Editor F. Beg. *(Corresponding author: A. P. Shah.)*

A. P. Shah and G. V. Dowhan are with the Applied Physics Program, University of Michigan, Ann Arbor, MI 48109 USA (e-mail: akashah@umich.edu).

B. J. Sporer and N. M. Jordan are with the Nuclear Engineering and Radiological Sciences Department, University of Michigan, Ann Arbor, MI 48109 USA.

K. W. Elliott and M. Krishnan are with Alameda Applied Sciences Corporation, Oakland, CA 94611 USA.

R. D. McBride is with the Applied Physics Program and the Nuclear Engineering and Radiological Sciences Department, University of Michigan, Ann Arbor, MI 48109 USA.

Color versions of one or more figures in this article are available at https://doi.org/10.1109/TPS.2024.3436054.

Digital Object Identifier 10.1109/TPS.2024.3436054

I. Introduction

Z-PINCHES can efficiently manufacture high-power x-rays and fusion neutrons, and understanding this process is crucial to various scientific aspirations in nuclear fusion [1], [2], [3], [4], material properties [5], [6], radiation science [7], [8], and laboratory astrophysics [9]. A z-pinch results from the axisymmetric compression of a plasma. A high-amplitude fast-rising voltage pulse from the discharging capacitors of a pulsed power device (i.e., a Marx generator or a linear transformer driver (LTD) [10], [11], [12], [13]) ionizes a "load," allowing it to conduct the current pulse in the axial direction. Using Ampère's law, this results in an azimuthal magnetic field. The axial current and azimuthal self-magnetic field produce an inward-pointing Lorentz force, which drives the plasma to the axis of symmetry, where it is further compressed.

A gas-puff z-pinch is an example of a specific type of load configuration—a *column of gas* is pinched [14], [15], [16], [17], [18], [19] by the pulsed power device (other load hardware configurations include wire arrays [20], [21] and solid liners [22]). The gas puff is delivered by a nozzle and fast-valve assembly. Multiple nozzles and fast-valve assemblies can be used to create load configurations with nested columns [23]. The radii and gas densities of these columns need to be determined as only a specific set of parameters can be efficiently pinched (i.e., an under-massed load will implode too early, before peak current has been achieved, while an over-massed load will not implode due to its inertia).

This article presents the design, fabrication, and initial testing of the gas-puff z-pinch system developed for the 0.5–1-MA, 100–250-ns MAIZE LTD [24] at the University of Michigan. Here, we describe the development of the nozzle and fast-valve load hardware; the transmission lines developed to accommodate the load hardware on MAIZE; the gas delivery system; the electrical control and monitoring system; and the diagnostic suite developed to monitor the implosion dynamics, x-ray yields, and neutron yields produced on the facility.

II. Initial Considerations

Developing a gas-puff z-pinch requires that we first establish parametric constraints on the density distribution of the gas in the load, such that its implosion time is roughly equivalent to the current pulse rise time to maximize the machine energy delivered to the stagnating plasma column [25]. The density of the load needs to be tailored to implode when the MAIZE current pulse peaks (i.e., between 100 and 250 ns). An over-massed load will implode late in time, while an under-massed

load will implode earlier in time, both resulting in inefficient coupling of driver energy to the z-pinch. Such timing considerations inform the nozzle design (i.e., the nozzle radius and gas pressure in the fast valve), which determines the density distribution of the gas in the load.

In addition to optimizing delivery of driver energy to the plasma, judicious selection of the density distribution can help in stabilizing the z-pinch. Z-pinches are afflicted by the magneto-Rayleigh–Taylor (MRT) instability [26], which is detrimental to achieving a stable and reproducible gas-puff z-pinch [27], [28]. Mitigating the growth of the MRT instability can be achieved using tailored density profiles [29] and multispecies implosions [16], [30], [31]. Both these instability mitigating methods require multiple nozzles in concentric shells to form a load of nested columns. A density profile with $\partial\rho(r,z)/\partial r$ sufficiently less than zero, such that the imploding shell does not accelerate, will stabilize MRT. One of the ways in which this can be achieved is by fielding a lighter outer shell, which implodes onto a heavier inner shell. Additionally, multispecies gas-puff z-pinches use an outer shell gas species with higher mass number than that of the gas in the inner shells. These have been experimentally shown to reduce MRT instability modes in addition to promoting yield reproducibility.

In evaluating possible configurations, it was decided that a triple-nozzle system (a central jet surrounded by two concentric shells) would be an appropriate testbed for gas-puff z-pinches on MAIZE, as has been implemented on other drivers [27], [28], [30]. The mass density can be adjusted such that it is highest in the central jet, lower in the inner shell, and lower yet in the outer shell. Additionally, the gas species for each nozzle can be uniquely selected to implode a high-Z gas (such as argon or neon) onto a low-Z gas (such as deuterium). The radii of the triple-nozzle system are informed by similar experiments at peer institutions, whereas the gas pressure in the fast valve has to be selected to best implode on MAIZE. As such, we have developed a simple 0-D voltage-driven thin-shell model.

The thin-shell model couples the implosion dynamics of the z-pinch to the driver circuit as shown in Fig. 1. This coupling is of particular importance when considering low-impedance drivers, such as single-cavity LTDs (i.e., MAIZE). The changing load impedance during the course of an implosion can reduce the output current of the driver, to the detriment of the z-pinch experiment. The voltage-driven model was used to determine the gas density distribution in the load and, by extension, the gas pressures in the fast valve that ultimately forms the load.

We consider separately the implosion of the two concentric shells of the gas-puff experiment to explore possible nozzle radii and mass distributions. The outer shell is tested with $r_{\text{out}} = 2.3$ cm, $r_{\text{in}} = 2.1$ cm, and $\rho = 1.3 \times 10^{-6}$ g·cm^{-3}. Similarly, the inner shell is tested with $r_{\text{out}} = 1.0$ cm, $r_{\text{in}} = 0.9$ cm, and $\rho = 20 \times 10^{-6}$ g·cm^{-3}. Here, r_{out} is the radius of the outer surface of the shell, while r_{in} is the radius of the inner surface of the shell. The model assumes that the mass distribution in the shell is collected at the outer surface, to which the model applies the driving magnetic pressure. Both

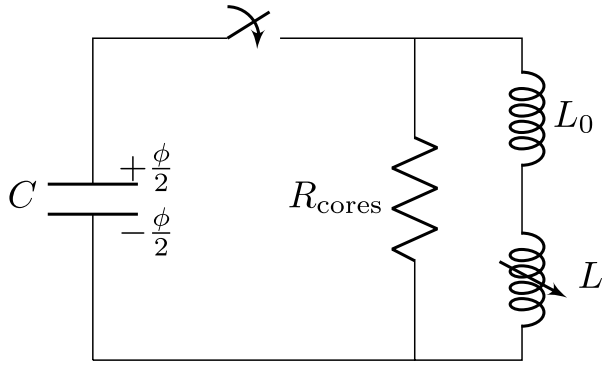

Fig. 1. Equivalent circuit for MAIZE coupled to a gas-puff z-pinch load. MAIZE consists of total capacitance, $C = 800$ nF, with a potential difference, $\phi = 120$ kV; machine inductance, $L = 15$ nH; and parasitic losses in the ferromagnetic cores of the LTD cavity, $R_{\text{cores}} = 3\ \Omega$. The gas-puff load is given a time-dependent inductance of $L(t)$, which changes as the implosion progresses and is calculated based on the load geometry at each time step in the implosion.

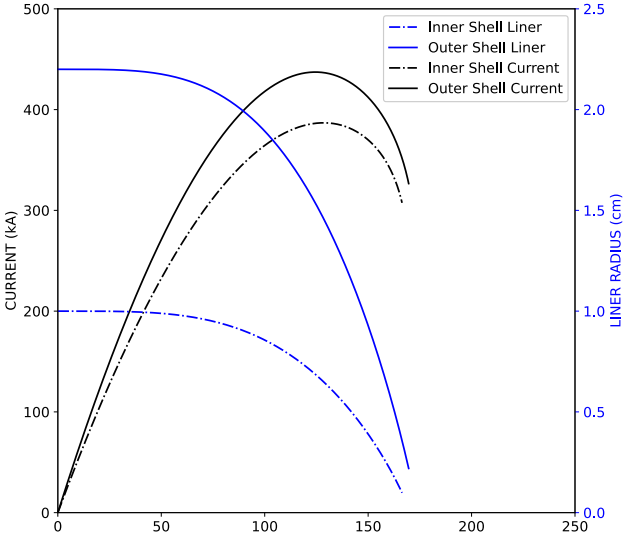

Fig. 2. Implosion dynamics of the outer (top) and inner (bottom) shells given MAIZE-like driver parameters. The outer shell is defined by $r_{\text{out}} = 2.2$ cm, $r_{\text{in}} = 2.0$ cm, and $\rho = 1.3 \times 10^{-6}$ g·cm^{-3}, while the inner shell is defined by $r_{\text{out}} = 1.0$ cm, $r_{\text{in}} = 0.9$ cm, and $\rho = 20 \times 10^{-6}$ g·cm^{-3}. The MAIZE capacitors are charged to ±60 kV. Each simulation is stopped when the implosion reaches a convergence ratio of ten, which is reasonable for gas-puff z-pinch implosions. The inner shell stagnates just before 170 ns, while the outer shell stagnates close to 175 ns.

the shells are given MAIZE-like driver parameters and they experience an implosion as shown in Fig. 2. These parameters result in the stagnation of the gas-puff z-pinch only slightly after peak current for each of the shells.

Note that fine adjustment of the pressures in the fast valve can be used to change these densities to better time the implosion in an experimental setting. Further note that while the model implodes each shell individually, adjustment of the gas pressures with both the shells present such that the average pressures are close to those described above will also result in a well-timed implosion on MAIZE.

III. System Hardware

Details of the nozzle and fast-valve hardware are discussed in Section III-A. Mounting this new hardware onto MAIZE required a redesign of specific sections of the transmission lines on MAIZE, and this process is discussed in Section III-B.

A CAD cut-out of the nozzle and fast-valve assembly, mounted onto the redesigned MAIZE transmission lines, is shown in Fig. 3. Additional auxiliary systems that support the experiment include: a gas manifold, which supplies the fast valve with gas that ultimately forms the load (see Section III-C); a fast-valve driver, which sends a current pulse to the fast valve so as to open and close it (see Section III-D); and a logic circuit, which ensures the presence of gas in the load region to avoid an inadvertent discharge of the MAIZE capacitors into an open circuit (see Section III-E). A summary schematic of the entire network is shown in Fig. 4.

A. Gas-Puff Nozzle and Fast Valve

The nozzle and fast-valve system function to produce a gas-puff load with a specific gas density distribution. These critical hardware components were manufactured by Alameda Applied Sciences Corporation (AASC) [32]. Currently, only the outer and inner shells are enabled on MAIZE, but the system was designed to incorporate the on-axis jet when needed.

Before the gas is injected into the load region of MAIZE, it is stored in the plenum, a section of the valve that is sealed off from the vacuum chamber. The plenum is evacuated to millitorr vacuum pressures and then pressurized by a gas line that is connected to a gas bottle through the gas manifold. This plenum pressure determines the load density profile. Each of the two valves (one for the outer shell and the other for the inner shell) in our system has a unique and independently pressurized plenum. For the valve to create a gas flow that results in a well-formed and symmetrical gas distribution, it must be opened and closed quickly.

A rapid response from the fast valve is achieved by driving a current pulse through a drive coil. Specifically, the valve is designed such that the coil presses against an O-ring on a metallic plate to seal the plenum from the downstream vacuum chamber. Driving a current with a sufficiently fast rise time through the inductive coil induces an eddy current in the metallic plate, which in turn induces a repulsive force between the coil and the metallic plate and causes the low-mass coil to accelerate away from the plate. This movement of the coil breaks the seal and allows gas to flow out of the plenum. As the current pulse decays, the restoring spring force returns the coil to its original position to reseal the plenum. Note that the nozzles and fast valve function similar to those developed for the Z facility [32].

As gas flows out of the plenum, it is forced through a throat plate, which is an aperture that defines an area of choked flow to accelerate the gas to supersonic velocities. For our system, a single throat plate with a separate aperture for each shell is used. The throat plate controls the azimuthal symmetry of the gas in the load region, and so it demands high precision in its fabrication. AASC used a laser to cut the throat plate in a thin stainless steel foil and then verified the tolerances by digitizing an image of the throat plate and using image processing software to ensure a high degree of azimuthal symmetry.

From the choked flow in the throat plate, the gas flows into the nozzle. The geometry of the nozzle pieces ensures an azimuthally uniform, nonturbulent gas flow and density distribution in the load region of the pulsed power device. The outer nozzle has an outer radius of 2.2 cm and an inner radius of 1.7 cm. The inner nozzle has an outer radius of 1.0 cm and an inner radius of 0.5 cm. Each nozzle is able to create a concentric gas target centered between its outer and inner radii. The nozzles have an inward tilt, which minimizes the divergence of the gas flow as it emerges from the nozzles into the vacuum chamber. Such a nondivergent and supersonic flow ensures that the gas rapidly and uniformly bridges the gap between the anode and cathode, completing the pulsed power circuit for a z-pinch experiment when MAIZE fires.

B. Transmission Line Redesign

For the MAIZE current pulse to flow along the transmission lines and through the gas-puff load, the nozzle and fast valve have to be physically integrated into the MAIZE circuit. This requires merging the nozzle and fast-valve assembly into the MAIZE transmission lines. In theory, a pulsed power device can be manufactured with only radial transmission lines. However, due to the azimuthal distribution of capacitors and switches, such a design severely limits diagnostic access to the load region. This problem is overcome by axially elevating the load region from the capacitor plane to a diagnostics plane, generally defined by the vacuum chamber ports [33].

The price for an axial translation of the transmission lines for diagnostic access is an increase in circuit impedance. Specifically, these elevated transmission lines have a higher inductance, which is a function of their geometry. MAIZE is a low-impedance driver, so it is important that the transmission lines be designed such that their inductance is minimized. An optimized power feed is curved, which can be reasonably approximated by a straight conical feed [34]. On MAIZE, the transmission lines from the capacitor outputs are primarily radial down to a radius of 15 cm, at which point they transition to the conical structure shown in Fig. 3.

The conical section of the power feed was redesigned to accommodate both the existing radial power feed and the newly fabricated nozzle and fast-valve assembly at the diagnostics plane. To this end, we evaluated the inductance of various conical transmission line geometries, whereby the overall transmission line structure is broken up into smaller, discrete sections that can be easily evaluated using the inductance formula for a coaxial transmission line; the partial inductances from the discrete sections are then summed to find the total inductance of the structure. We tested a range of various geometries and selected one after accounting for inductance and ease of manufacturing (see Fig. 5). The selected geometry has a calculated inductance of 7 nH. Note that this is only the inductance of the conical section—it must be added to the inductance of the rest of the MAIZE discharge circuit, which includes the load, the switches, and the radial section of the transmission lines. Further note that this low-inductance transmission line is used for other experiments on MAIZE, as it improves the efficiency of the pulsed power device.

On MAIZE, the nozzle and fast-valve system is mounted on the conical section of the cathode. The nozzle defines the cathode plane of the gas-puff z-pinch, and a metallic mesh,

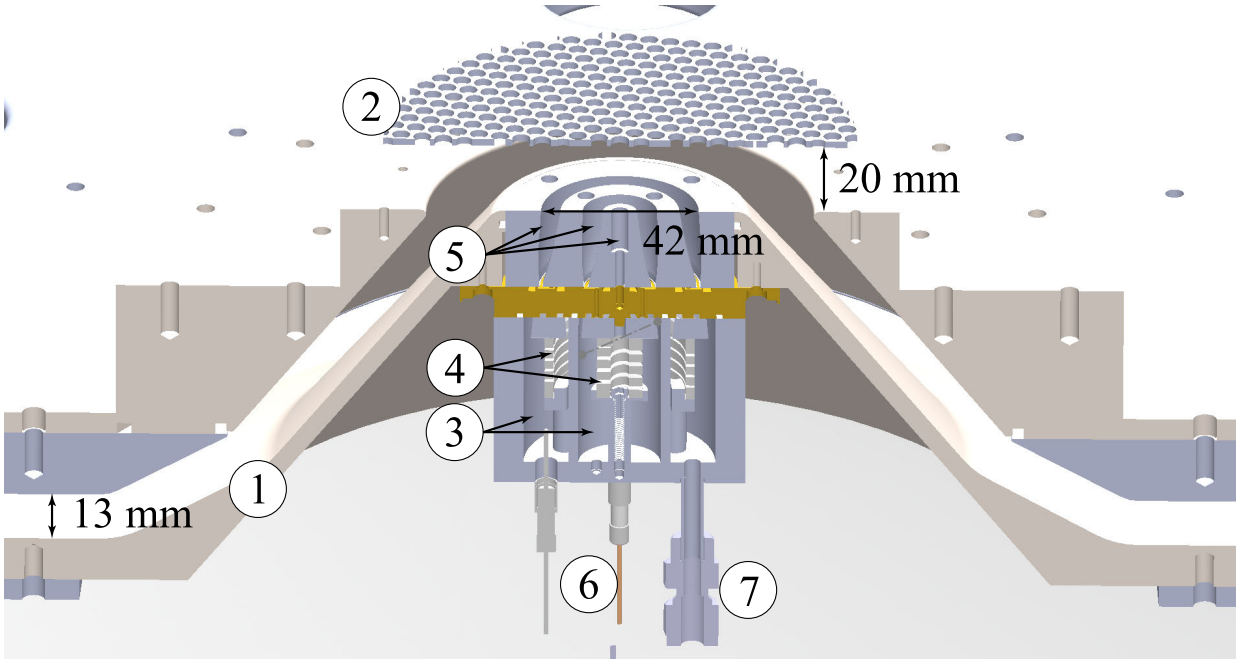

Fig. 3. CAD cross section rendering of the MAIZE load region. 1—Redesigned MAIZE conical transmission lines with a 13-mm gap along their entire length. 2—Anode metallic mesh 20 mm above the cathode. 3—Outer shell and inner shell plena. 4—Outer shell and inner shell inductive coil. 5—Outer shell, inner shell, and central jet nozzles. 6—Inner shell electrical connection. 7—Outer shell gas connection. Note that the central jet plenum and inductive coil can be installed in the future.

located 2-cm above the cathode plane, defines the anode plane. The transmission line design maintains a conservative 13-mm gap between the anode and the cathode. A conservative gap spacing helps ensure that stray gas that circulates into the power feed during a gas-puff shot sequence will not shunt the large A-K gap in the transmission lines and reduce the driver current at the load. Note that due to the high frequency of the discharge, the MAIZE current flows along the nozzle surface during a shot and can damage the nozzle due to localized heating and arcing. In practice, the nozzle is refurbished or even replaced after approximately 250 shots on MAIZE.

C. Gas Manifold

The nozzle and fast valve must be supplied with gas, which ultimately goes on to form the experimental load for the gas-puff z-pinch. The gas manifold is the control unit that supplies gas to the two plena of the two corresponding fast valves (one plenum for each shell). As such, the gas manifold has two inputs and two outputs. Gas bottles supply the inputs of the manifold and are selected for the gas species desired for each particular shell.

Each of the inputs in the gas manifold flows through a valve to the output. Opening the output valve allows gas to flow to the plenum of the fast valve; leaving the output valve open for a sufficiently long time ($\approx$10 s) will equalize the pressure of the plenum to that set on the output of the gas bottle. A pressure gauge is placed on the output end of the manifold to indicate the gas pressure in the plenum. On each of the plena outputs in the manifold, two additional parallel paths are constructed for the gas from the bottles to flow along: one through a valve to a vacuum roughing pump, and the other through a separate valve to atmosphere. The former allows the plena to be pumped down, and the latter allows the plena to be vented to atmosphere. Note that we use aluminum lines from the output of the gas manifold to the fast valve to allow the lines to be pumped down below atmospheric pressure and reduce outgassing associated with plastic lines.

When establishing the fast-valve pressures using the gas manifold, we first close off the output valves to isolate the gas bottle from the plena. We then evacuate the plena by opening the roughing valves. We open the output valves to fill the plena with the desired gas. Repeated pumping down and filling of the plena with the desired gas is advised to dilute trace contaminants such as air or previously used gas species. After sufficient flushing out of contaminants, the output valve and roughing valve are tweaked to achieve the desired plena pressure. After the experiment is completed, the vent valve can be used to bring the plena to atmosphere. The gas manifold allows for precise control of the plena pressures, which in turn determines the desired density distribution of the gas-puff z-pinch.

D. Valve Driver

A current is supplied to the fast valves with a separate high-voltage capacitor discharge. This current pulse profile is characterized by the impedance of the inductive coil in the valve. Due to the geometry of the valves for the inner and outer shells, the inductive coils, which form the seals in their respective shell, have different inductances. A unique capacitor charge is required to achieve proper opening and closing of each of the two valves, and each valve has its own driver and high-voltage power supply for independent control.

Note that the cables connecting the drivers to the nozzle and fast-valve system, which is mounted onto the cathode in the vacuum chamber, create an alternate and undesirable current path that conducts a fraction of the MAIZE pulse back to

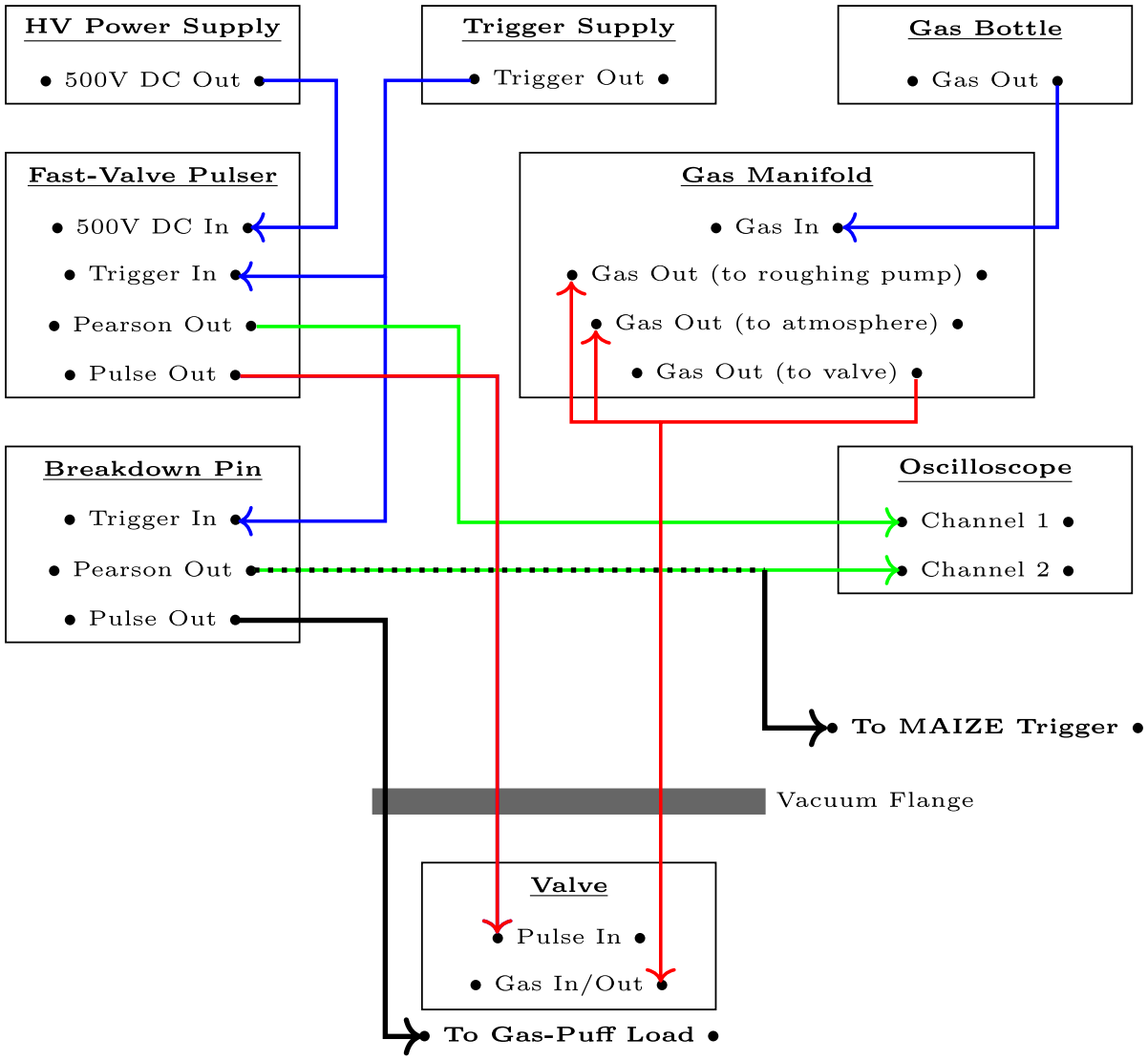

Fig. 4. Schematic of the overall gas-puff z-pinch system on MAIZE, showing how the various subsystems are connected. Note that two separate HV power supplies and fast-valve drivers are used to drive each valve independently. Additionally, the gas manifold has a unique input and output for each of the two fast valves. The output of the breakdown pin circuit feeds through a Pearson coil, the signal of which is used to trigger MAIZE and its diagnostic suite with the appropriate time delays.

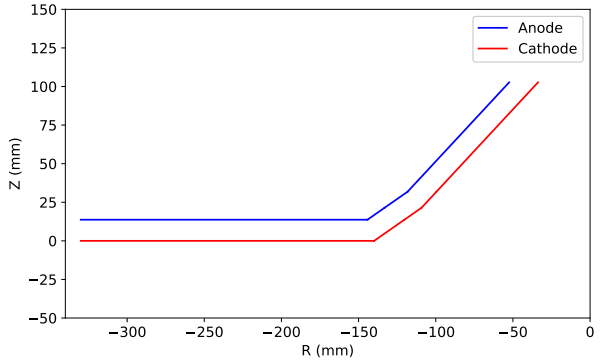

Fig. 5. Cross-sectional view of the conical MAIZE transmission lines, designed to minimize inductance and integrate into MAIZE's radial transmission lines. This 7-nH design was ultimately selected for use with the new gas-puff nozzles and fast valves (see Fig. 3).

the drivers. To avoid this, we ensure that the MAIZE circuit, including the nozzle and fast-valve system, is inductively isolated from the valve drivers by feeding the power and gas lines that supply the nozzles and fast valves through a large metallic coil. The power and gas lines are wrapped in a metallic over-braid from the metallic coil all the way to the MAIZE vacuum chamber.

E. Logic Circuit

Prior to discharging the MAIZE capacitors through the double-shell structure of the gas in the load region, we must independently verify the presence of the gas. This verification provides the breakdown logic for MAIZE to fire and is required to ensure that the pulsed power device does not discharge into an open circuit. Firing MAIZE into an open circuit can dramatically reduce the lifetime of various electrical components.

For the MAIZE gas puff, the breakdown logic is provided by the discharge of a 10-kV, 1-μF capacitor through the peripheral neutral gas above the anode mesh (see Fig. 6). The positively charged capacitor is discharged by closing a spark-gap switch to ground, which results in a negative-polarity pulse. This negative pulse is coupled to the gas through a thin metallic

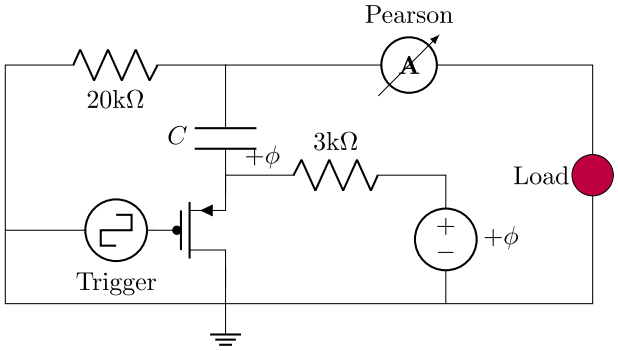

Fig. 6. Circuit schematic of the breakdown logic generator. The generator relies on a low-side spark gap to switch a positively charged capacitor to ground. The capacitor is charged to $\phi = 7$ kV. This results in a current pulse through the gas after the nozzles fire, which is measured by the Pearson coil, and which provides the trigger signal for MAIZE to fire. Such a circuit ensures that MAIZE is not discharged into an open circuit when there is no gas present.

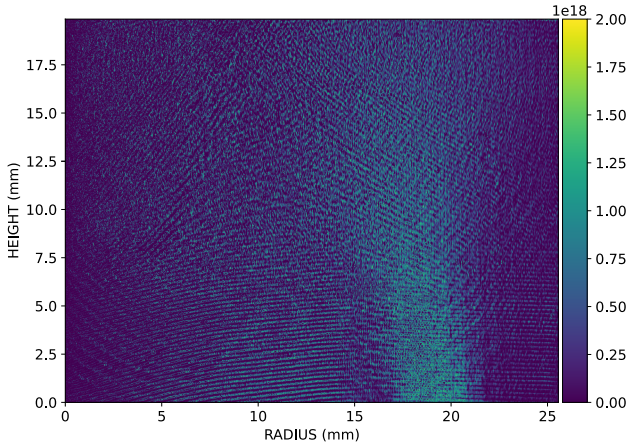

Fig. 7. Fourier unfold of an interferogram showing the number density (cm^{-3}) of a puff of gas from the outer shell of the gas-puff nozzle. A sequence of these images were obtained at various times and with the nozzles at various pressures and quantified to make the plots shown in Fig. 8.

wire, which sits above the anode return current structure. The height that the wire sits at is empirically selected to ensure a breakdown of the gas between the wire and the MAIZE anode. A Pearson coil on the output of the logic circuit provides the trigger signal for MAIZE. This logic circuit can only fire if there is a specific amount of gas through which it can discharge.

IV. Diagnostics Suite

The MAIZE facility includes a range of imaging diagnostics (e.g., laser shadowgraphy, visible light self-emission imaging, and extreme ultraviolet self-emission imaging), x-ray diagnostics (e.g., a bolometer and multiple polycyrstalline diamond detectors), and neutron diagnostics (e.g., bubble detectors and a beryllium probe detector [35]). For testing the gas-puff z-pinch system on MAIZE, a 2-D Mach–Zehnder interferometer was developed to characterize the initial neutral gas density distribution in the load region on MAIZE. The implosion trajectories were mapped with visible light and extreme ultraviolet self-emission imaging. The polycrystalline diamond (PCD) detectors were fielded as Ross filter pairs to quantify the x-ray spectra emitted from the pinch. Additionally, neutron bubble detectors were fielded to measure the fusion neutron yield from deuterium pinches.

We set up a 2-D Mach–Zehnder interferometer with a 532-nm wavelength, 2-ns pulsewidth laser beam, which is expanded from 5 to 60 mm, split into two equal path lengths, and recombined to form an interference pattern. One of the split paths traverses the gas-puff experiment to form the probe beam while the other forms the reference beam. The probe beam experiences a phase change as it crosses the region of a high index of refraction due to the gas in the load region relative to the reference beam. The interference pattern is imaged with a Canon XTi Rebel DSLR camera. An interference image before and during the firing of the gas puff is acquired. A computer script was written to analyze the interference patterns to extract the density distribution in the load region via a Fourier unfold (see Fig. 7). We used the interferometer to determine the gas-puff densities that result from particular time delays and fast-valve pressures (see Section V-A).

We set up an array of four PCDs to help quantify the x-ray spectrum of the output radiation of the z-pinch. In particular, we used PCDs with a 2.5-μm copper and 50-μm polypropylene filter; a 4-μm silver filter; a 5-μm molybdenum filter; and a 10-μm titanium and 50-μm polypropylene filter. Each filter has a unique transparency profile to incoming x-ray photon energies. Looking at the difference in the amplitude between two PCDs with different filters allows us to acquire spectral information about the x-rays. For instance, the difference between the signal on the PCD with the 4-μm silver filter and on the PCD with the 5-μm molybdenum filter gives the x-rays in the 2.5–3.4-keV range, which should capture the radiation of the argon K-shell line in the 3.0–3.2-keV range.

We also set up an array of neutron bubble detectors and a beryllium probe detector to quantify the neutron output for when we pinch deuterium in the gas-puff z-pinch. Pinching deuterium can result in nuclear fusion reactions, which results in the output of fusion neutrons. Bubble detectors make use of pockets of super-heated liquid in an epoxy. Neutrons incident on these pockets perturb the liquid, which results in its phase change to a gas, forming a bubble in the epoxy. Counting the bubbles in the detector after a pinch event quantifies the neutron yield. The beryllium probe detector relies on the activation of beryllium to form an unstable ^{6}He isotope, the decay of which releases beta electrons. These are absorbed in a plastic scintillator, and subsequent visible light pulses are counted. The count from these light pulses is correlated to the neutron yield from the pinch.

The complete diagnostics suite on MAIZE allows for a comprehensive analysis of the gas-puff z-pinch from the initial gas density distribution, through the implosion process, to the x-ray and neutron output.

V. System Demonstration

A. Fast Valves and Nozzle Characterization

With the gas-puff z-pinch experimental hardware built and integrated into the MAIZE pulsed power generator, the next step is to characterize the initial density distribution of the system as a function of its parameters (i.e., the timing, pressure,

and gas species used). Each of the inner and outer shells of the gas-puff hardware must be separately characterized.

Timing experiments were carried out by maintaining a constant plenum pressure with argon and varying the timing between when the fast valve fires and when the interference pattern was acquired. The plenum pressure was set to 10 psig for both the inner and outer shells. Target formation was observed with a peak density occurring between the outer and inner radii of each of the shells. The full-width-at-half maximum of the peak was used to define the density distribution in the shell. Note that the gas flow from each nozzle was slightly divergent, so the density values were obtained by averaging the density distributions axially within a 1-cm-tall window centered 0.5 cm above the cathode plane.

For the outer shell, the gas target formed approximately 600 μs after the fast valve of the outer shell fired, peaking at 800 μs, and then decreasing. We then selected 700 μs after the fast valve of the outer shell fires as the time to discharge MAIZE. Similarly, for the inner shell, the gas target formed approximately 300 μs after the fast valve fired, peaking at 500 μs, and maintaining a steady-state flow. We then selected 500 μs after the fast valve of the inner shell fires as the time to discharge MAIZE.

The pressure experiments were carried out by maintaining a constant timing, as determined by the timing experiments (i.e., 700 μs for the outer shell and 500 μs for the inner shell with argon), and varying the plenum pressures. For both the shells, there is less gas for both high and low pressures and more gas for intermediate pressures. This is explained by the fact that at very high pressures, there is more force holding the o-ring seal against the metallic plate that constitutes the fast valve, and so it does not open as much as in cases with lower gas pressures. On the other hand, at very low pressures, there is less gas that is puffed into the target region. The relationship between the plenum pressure and the density distribution is shown in Fig. 8. Note that the curves for deuterium density distribution were determined experimentally by firing MAIZE into various timing and pressure fills and matching the implosion dynamics to that of argon implosions.

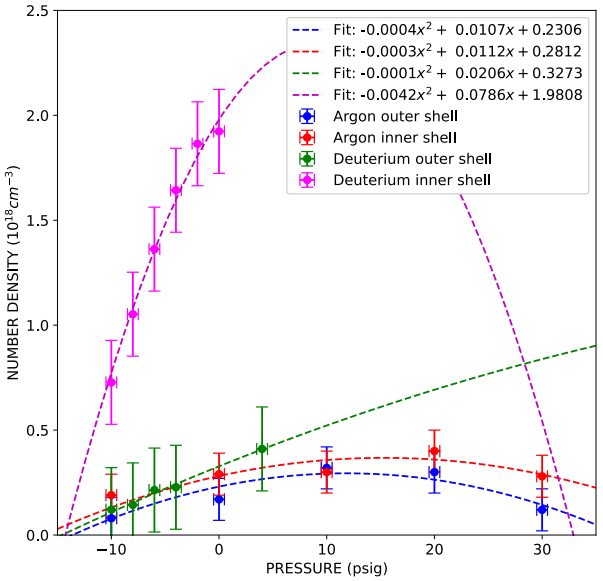

Fig. 8. Summary of interferometry results giving the relationship between the plenum pressure and the gas-puff neutral number density when MAIZE discharges for argon and deuterium for the outer and inner shells. Note that for these curves to hold for argon, density is measured 500 μs after the inner shell fast valve fires, and 700 μs after the outer shell fast valve fires, while for deuterium, density is measured 300 μs after the inner shell fast valve fires, and 500 μs after the outer shell fast valve fires.

B. Characteristic Implosions

Characteristic implosions of outer and inner shells of the gas-puff z-pinch with argon and deuterium are presented in Figs. 9 and 10, respectively. For the outer shell argon experiment with a mass density of 1.0×10^{-6} g·cm^{-3} (shot 2193), the peak current was 350 kA with the implosion stagnating at 290 ns. For the inner shell argon experiment with a mass density of 11×10^{-6} g·cm^{-3} (shot 2223), the peak current was 270 kA, with the implosion stagnating at 190 ns. For the outer shell deuterium experiment with a mass density of 1.6×10^{-6} g·cm^{-3} (shot 2304), the peak current was 330 kA with the implosion stagnating at 360 ns. For the inner shell deuterium experiment with a mass density of 13×10^{-6} g·cm^{-3} (shot 2297), the peak current was 310 kA, with the implosion stagnating at 220 ns.

Note that the simulations from Section II uniformly under-predict time to stagnation for the experimentally tested mass densities. Such behavior can be explained by a discrepancy in current distribution between the simulation and the experiment. The implosions in the simulations perfectly conduct the entirety of the current delivered to the target in an infinitely thin shell at the outer boundary of the pinch. A real experiment, however, is afflicted by imperfect delivery of machine current to the target and the result is a slower than the predicted implosion. The inner shell implosions for both argon and deuterium gas were better matched to simulations than the outer shell implosions, implying that the current delivery for the former was better optimized than the latter.

Additionally, the simulations are a 0-D approximation, whereas the experiments are 3-D objects and are subject to instabilities that affect implosion dynamics. Future experiments with more refined timing resolution (i.e., shorter interframe times) could be performed to measure instability growth rates. For now, using the course timing resolutions shown in Fig. 10, we can say that the instability growth rates are in the range of 0.01–0.02 ns^{-1}, which is comparable to similar experiments [36], [37], [38].

C. X-Ray and Neutron Yield

The bolometer indicates a soft x-ray yield of 410 ± 29 J for the outer shell experiment (shot 2193) and 630 ± 44 J for the inner shell experiment (shot 2223). With MAIZE charged to $\pm$60 kV, the stored energy is 5.7 kJ, which corresponds to a wall-plug efficiency of roughly 7.2% for the outer shell implosion and 11% for the inner shell implosion. Yields of up to 720 ± 50 J were measured with the inner shell (shot 2216) to give a wall-plug efficiency of 13%. The kinetic energy is calculated to be 110 ± 28 J for the outer shell experiment and 150 ± 38 J for the inner shell experiment. This result is analogous to wire-array z-pinches, which have

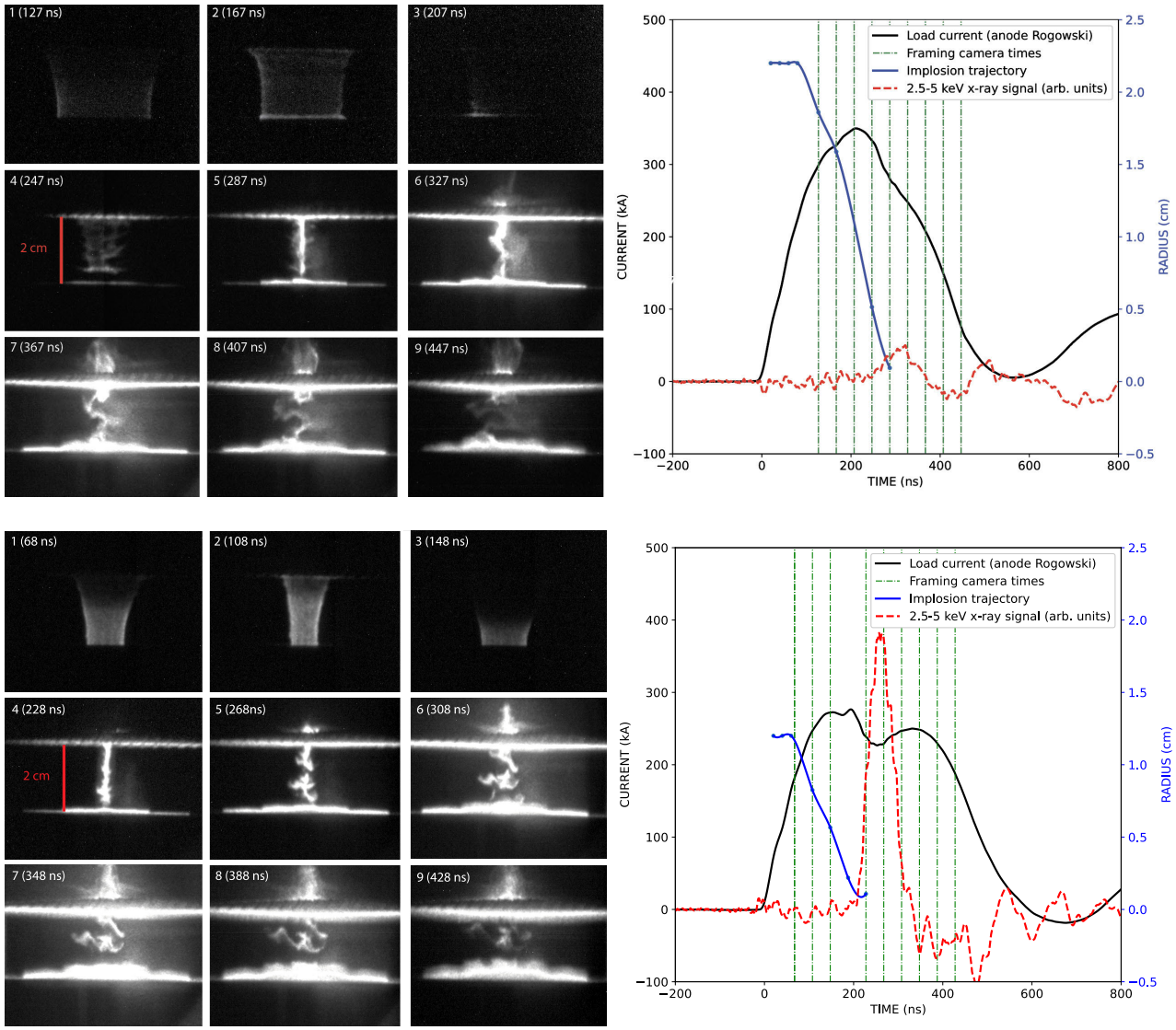

Fig. 9. Summary of results for an argon outer shell mass density of 1.0×10^{-6} g·cm^{-3} (shot 2193; top) and an argon inner shell mass density of 11×10^{-6} g·cm^{-3} (shot 2223; bottom). The sequence of images on the top and bottom left show the fast-framing camera images of the implosion (these are visible light self-emission images; frames 1–3 on the top have been digitally enhanced to better visualize the self-emission). The plots on the top and bottom right show the current pulse, timing of the fast-framing camera images, implosion trajectory based on the experimental data, and the argon K-shell signal in 2.5–5.0-keV range.

repeatedly produced x-ray yields four times greater than the kinetic energy of the implosion [39].

Fig. 9 also shows the trace of the difference between two PCD detectors: one with the 10-μm titanium and 50-μm polypropylene filter, and the other with the 5-μm molybdenum filter. This trace is correlated to x-ray energies between 2.5 and 5.0 keV, which contains the argon K-shell line. These traces show that the inner shell implosion was a more efficient source of argon K-shell emission than the outer shell. Note that both the bolometer and PCD measurements were not collimated to reject emission from above the anode grid, so some contribution from this region is expected, based on the image data presented in Figs. 9 and 10.

The bubble detectors did not detect any neutrons for the outer shell experiment (shot 2304). They detected a yield of $(4.8 \pm 0.5) \times 10^6$ neutrons for the inner shell experiment (shot 2297). More optimized yields of up to $(4.9 \pm 0.5) \times 10^8$ were measured with the inner shell (e.g., shot 2300). Furthermore, the neutron output observed was anisotropic with higher fluence observed on the z-pinch axis and lower fluence observed perpendicular to the z-pinch axis. Indeed, no neutrons were observed perpendicular to the z-pinch axis for the inner shell experiment (shot 2297). Such a spatial distribution suggests that the neutrons are beam target in origin, as opposed to thermonuclear, which is characterized by an isotropic spectrum [40].

D. Repetition Rate

This experimental setup has demonstrated a high repetition rate of >30 shots per day. Pulsed power driven z-pinch experiments often face a bottleneck in achieving a high daily shot rate: the destructive nature of the experiment requires that the user vent and open the vacuum chamber to replace the necessary target hardware. With a gas-puff system, the fast valve can be repeatedly triggered to create the load

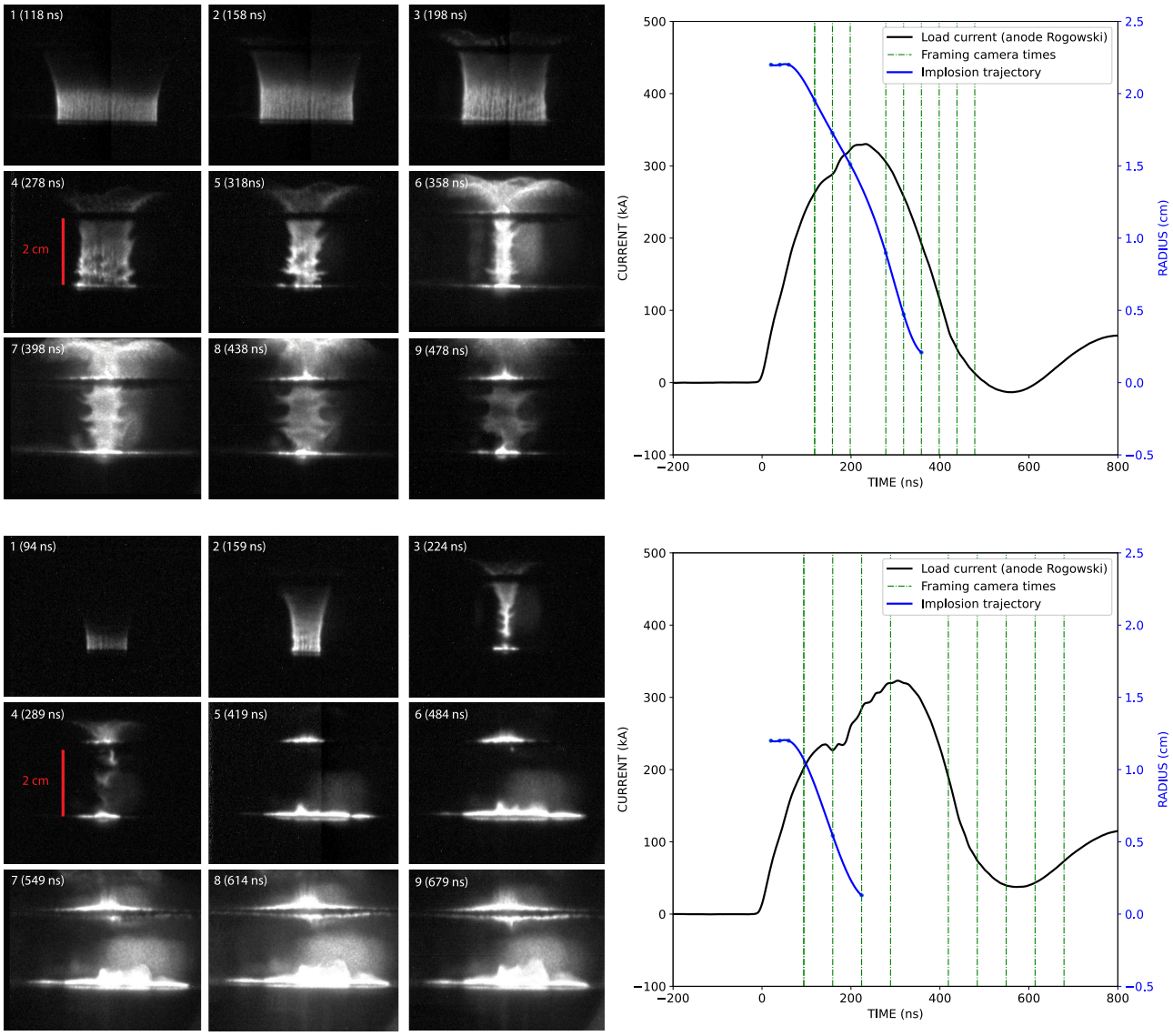

Fig. 10. Summary of results for a deuterium outer shell mass density of 1.6×10^{-6} g·cm^{-3} (shot 2304; top) and a deuterium inner shell mass density of 13×10^{-6} g·cm^{-3} (shot 2297; bottom). The sequence of images on the top and bottom left shows the fast-framing camera images of the implosion (these are visible light self-emission images). The plots on the top and bottom right show the current pulse, timing of the fast-framing camera images, and implosion trajectory based on the experimental data.

without having to interfere with the vacuum. In practice, sufficient time is needed for the background gas vacuum pressure to equilibrate to nominal shot conditions. During this time, the spark-gap switches are vented to expel possible contaminants and are repressurized. A subsequent experiment can be carried out within minutes of its predecessor. We have carried out 34 shots in a single day (shots 2275–2308). The system is capable of approximately 50 shots per day. With certain automation upgrades, this can be further extended to approximately 80 shots per day. This capability allows users to carry out wide parameter scans and obtain statistically significant results.

VI. Summary, Conclusion, and Future Work

This article discusses the development of a gas-puff z-pinch experimental platform for the 0.5–1-MA, 100–250-ns MAIZE LTD at the University of Michigan. In particular, a triple-shell gas-puff fast valve and nozzle has been developed, of which the outer shell and inner shell are currently operational. The outer shell (inner shell) creates a hollow cylindrical shell with an outer radius of 2.2 cm (1.0 cm) and an inner radius of 1.7 cm (0.5 cm). The system has been integrated into MAIZE with redesigned high-power, low-inductance, magnetically insulated transmission lines. Auxiliary systems that drive the fast-valves and supply gas to the system have also been developed and integrated. New diagnostics to help characterize the initial conditions and to measure x-ray and neutron yields have been developed and fielded.

With MAIZE charged to ±60 kV (to give stored energy of 5.7 kJ), the system has produced x-ray yields of 720 ± 50 J, with argon pinches, and neutron yields of $(4.9 \pm 0.5) \times 10^8$, with deuterium pinches. A high repetition rate of upward of 30 shots per day has also been demonstrated. Scientific studies using this new experimental capability are presently underway. In particular, parameter scans have been conducted to test varying load densities on the implosion trajectories, instabil-

ity development, and x-ray and neutron yield. Additionally, studies examining the effects of preionization on the gas-puff z-pinch have been conducted. These studies will be the subject of future publications.

ACKNOWLEDGMENT

The authors would like to thank Dr. Sophia Rocco and Dr. Phil Coleman for helpful discussions in the development of the experiment and analysis of the data presented here.

REFERENCES

[1] S. A. Slutz et al., "Pulsed-power-driven cylindrical liner implosions of laser preheated fuel magnetized with an axial field," *Phys. Plasmas*, vol. 17, no. 5, May 2010, Art. no. 056303, doi: 10.1063/1.3333505.

[2] M. E. Cuneo et al., "Magnetically driven implosions for inertial confinement fusion at Sandia National Laboratories," *IEEE Trans. Plasma Sci.*, vol. 40, no. 12, pp. 3222–3245, Dec. 2012, doi: 10.1109/TPS.2012.2223488.

[3] S. A. Slutz and R. A. Vesey, "High-gain magnetized inertial fusion," *Phys. Rev. Lett.*, vol. 108, no. 2, Jan. 2012, Art. no. 025003, doi: 10.1103/PhysRevLett.108.025003.

[4] M. R. Gomez et al., "Experimental demonstration of fusion-relevant conditions in magnetized liner inertial fusion," *Phys. Rev. Lett.*, vol. 113, Oct. 2014, Art. no. 155003, doi: 10.1103/PhysRevLett.113.155003.

[5] R. W. Lemke et al., "Probing off-Hugoniot states in Ta, Cu, and Al to 1000-GPa compression with magnetically driven liner implosions," *J. Appl. Phys.*, vol. 119, no. 1, 2016, Art. no. 015904, doi: 10.1063/1.4939675.

[6] M. R. Martin et al., "Solid liner implosions on Z for producing multi-megabar, shockless compressions," *Phys. Plasmas*, vol. 19, no. 5, 2012, Art. no. 056310, doi: 10.1063/1.3694519.

[7] J. E. Bailey et al., "Radiation science using Z-pinch X rays," *Phys. Plasmas*, vol. 9, no. 5, pp. 2186–2194, 2002, doi: 10.1063/1.1459454.

[8] G. A. Rochau et al., "Radiating shock measurements in the Z-pinch dynamic hohlraum," *Phys. Rev. Lett.*, vol. 100, Mar. 2008, Art. no. 125004, doi: 10.1103/PhysRevLett.100.125004.

[9] G. A. Rochau et al., "ZAPP: The Z astrophysical plasma properties collaboration," *Phys. Plasmas*, vol. 21, no. 5, 2014, Art. no. 056308, doi: 10.1063/1.4875330.

[10] B. M. Koval'Chuk et al., "Fast primary storage device utilizing a linear pulse transformer," *Russian Phys. J.*, vol. 40, no. 12, pp. 1142–1153, Dec. 1997, doi: 10.1007/BF02524302.

[11] A. A. Kim, B. M. Kovalchuk, E. V. Kumpjak, and N. V. Zoi, "0.75 MA, 400 ns rise time LTD stage," in *Proc. 12th IEEE Int. Pulsed Power Conf.*, vol. 2, Jun. 1999, pp. 955–958.

[12] A. A. Kim et al., "Development and tests of fast 1-MA linear transformer driver stages," *Phys. Rev. Special Topics—Accel. Beams*, vol. 12, May 2009, Art. no. 050402, doi: 10.1103/PhysRevSTAB.12.050402.

[13] J. D. Douglass et al., "100 GW linear transformer driver cavity: Design, simulations, and performance," *Phys. Rev. Accel. Beams*, vol. 21, Dec. 2018, Art. no. 120401, doi: 10.1103/PhysRevAccelBeams.21.120401.

[14] J. Shiloh, A. Fisher, and N. Rostoker, "Z pinch of a gas jet," *Phys. Rev. Lett.*, vol. 40, pp. 515–518, Feb. 1978, doi: 10.1103/PhysRevLett.40.515.

[15] P. G. Burkhalter, J. Shiloh, A. Fisher, and R. D. Cowan, "X-ray spectra from a gas-puff Z-pinch device," *J. Appl. Phys.*, vol. 50, no. 7, pp. 4532–4540, Jul. 2008, doi: 10.1063/1.326560.

[16] J. Bailey, Y. Ettinger, A. Fisher, and N. Rostoker, "Gas-puff Z pinches with D2 and D2-Ar mixtures," *Appl. Phys. Lett.*, vol. 40, no. 6, pp. 460–462, Mar. 1982, doi: 10.1063/1.93148.

[17] A. V. Shishlov et al., "Long time implosion experiments with double gas puffs," *Phys. Plasmas*, vol. 7, no. 4, pp. 1252–1262, Apr. 2000, doi: 10.1063/1.873936.

[18] R. B. Spielman et al., "Z-pinch experiments on Saturn at 30 TW," in *Proc. AIP Conf.*, vol. 195, Dec. 1989, pp. 3–16, doi: 10.1063/1.38844.

[19] F. Zucchini et al., "First argon gas puff experiments with 500 ns implosion time on Sphinx driver," in *Proc. AIP Conf.*, Jan. 2009, vol. 1088, no. 1, pp. 247–250, doi: 10.1063/1.3079740.

[20] Y. Li et al., "Influence of insulating coating on aluminum wire explosions," *Phys. Plasmas*, vol. 21, Nov. 2014, Art. no. 102513.

[21] D. Ampleford et al., "Opacity and gradients in aluminum wire array Z-pinch implosions on the Z pulsed power facility," *Phys. Plasmas*, vol. 21, Mar. 2014, Art. no. 031201.

[22] D. Sinars et al., "Measurements of magneto-Rayleigh–Taylor instability growth during the implosion of initially solid Al tubes driven by the 20-MA, 100-ns Z facility," *Phys. Rev. Lett.*, vol. 105, Oct. 2010, Art. no. 185001.

[23] C. Deeney, C. Coverdale, and M. Douglas, "A review of long-implosion-time Z pinches as efficient and high-power radiation sources," *Laser Part. Beams*, vol. 19, no. 3, pp. 497–506, 2001.

[24] R. M. Gilgenbach et al., "MAIZE: A 1 MA LTD-driven Z-pinch at The University of Michigan," in *Proc. AIP Conf.*, 2009, vol. 1088, no. 1, pp. 259–262, doi: 10.1063/1.3079742.

[25] T. Miyamoto, "Analysis of high-density Z-pinches by a snowplow energy equation," *Nucl. Fusion*, vol. 24, no. 3, pp. 337–348, Mar. 1984, doi: 10.1088/0029-5515/24/3/008.

[26] D. Ryutov, M. Derzon, and M. Matzen, "The physics of fast Z pinches," *Rev. Mod. Phys.*, vol. 72, pp. 167–223, 2000.

[27] H. Sze et al., "Efficient radiation production in long implosions of structured gas-puff Z pinch loads from large initial radius," *Phys. Rev. Lett.*, vol. 95, Sep. 2005, Art. no. 105001, doi: 10.1103/PhysRevLett.95.105001.

[28] R. J. Commisso et al., "Energetics of a long-implosion-time, 12-cm-diameter argon-gas-puff Z pinch at 6.5 MA," in *Proc. 16th IEEE Int. Pulsed Power Conf.*, vol. 2, Jun. 2007, pp. 1773–1779.

[29] A. L. Velikovich, F. L. Cochran, and J. Davis, "Suppression of Rayleigh–Taylor instability in Z-pinch loads with tailored density profiles," *Phys. Rev. Lett.*, vol. 77, pp. 853–856, Jul. 1996, doi: 10.1103/PhysRevLett.77.853.

[30] N. Qi et al., "Study of gas-puff Z-pinches on COBRA," *Phys. Plasmas*, vol. 21, no. 11, Nov. 2014, Art. no. 112702.

[31] R. Cherdizov, V. Kokshenev, N. Kurmaev, A. Shishlov, and S. Vagaytsev, "Optimization of double shell hybrid gas-puff with outer plasma shell for efficient generation of K-shell radiation in the microsecond implosion regime," in *Proc. 8th Int. Congr. Energy Fluxes Radiat. Effects*, Nov. 2022, pp. 148–153.

[32] M. Krishnan et al., "Architecture, implementation, and testing of a multiple-shell gas injection system for high current implosions on the Z accelerator," *Rev. Sci. Instrum.*, vol. 84, no. 6, Jun. 2013, Art. no. 063504, doi: 10.1063/1.4809511.

[33] P. C. Campbell et al., "Diagnostic and power feed upgrades to the MAIZE facility," *IEEE Trans. Plasma Sci.*, vol. 46, no. 11, pp. 3973–3981, Nov. 2018, doi: 10.1109/TPS.2018.2858796.

[34] R. D. McBride et al., "A primer on pulsed power and linear transformer drivers for high energy density physics applications," *IEEE Trans. Plasma Sci.*, vol. 46, no. 11, pp. 3928–3967, Nov. 2018, doi: 10.1109/TPS.2018.2870099.

[35] C. L. Ruiz et al., "Novel beryllium-scintillator, neutron-fluence detector for magnetized liner inertial fusion experiments," *Phys. Rev. Accel. Beams*, vol. 22, Apr. 2019, Art. no. 042901, doi: 10.1103/PhysRevAccelBeams.22.042901.

[36] P. W. L. de Grouchy et al., "Observations of the magneto-Rayleigh–Taylor instability and shock dynamics in gas-puff Z-pinch experiments," *Phys. Plasmas*, vol. 25, no. 7, Jul. 2018, Art. no. 072701, doi: 10.1063/1.5032084.

[37] E. S. Lavine et al., "Implosion dynamics of triple-nozzle gas-puff Z pinches on COBRA," *Phys. Plasmas*, vol. 28, no. 2, Feb. 2021, Art. no. 022703, doi: 10.1063/5.0030936.

[38] F. Conti, J. Narkis, A. Williams, V. Fadeev, and F. N. Beg, "Dynamics and energy coupling of gas puff Z-pinches on a fast linear transformer driver," *J. Appl. Phys.*, vol. 130, no. 2, Jul. 2021, Art. no. 023301, doi: 10.1063/5.0051335.

[39] M. G. Haines, P. D. LePell, C. A. Coverdale, B. Jones, C. Deeney, and J. P. Apruzese, "Ion viscous heating in a magnetohydrodynamically unstable Z pinch at over 2×10^9 Kelvin," *J. Appl. Phys.*, vol. 96, Feb. 2006, Art. no. 075003, doi: 10.1103/PhysRevLett.96.075003.

[40] A. L. Velikovich et al., "Z-pinch plasma neutron sources," *Phys. Plasmas*, vol. 14, no. 2, Feb. 2007, Art. no. 022701, doi: 10.1063/1.2435322.